Rev. Adv. Mater. Sci. 29 (2011) 105-125

MICROMECHANISMS FOR IMPROVED FRACTURE TOUGHNESS IN NANOCERAMICS

I.A. Ovid'ko[1,2] and A.G. Sheinerman[1]

[1]Institute of Problems of Mechanical Engineering, Russian Academy of Sciences, Bolshoj 61, Vasil. Ostrov, St. Petersburg 199178, Russia
[2]Department of Mathematics and Mechanics, St. Petersburg State University, Universitetskii pr. 28, Staryi Petergof, St. Petersburg 198504, Russia

Received: October 11, 2011

Abstract. We present an overview of experimental data, computer simulations and theoretical models on crack growth and its stoppage in nanocrystalline ceramics. The focuses are placed on micromechanisms for improvement of fracture toughness in such ceramic materials. Special attention is paid to theoretical models describing various modes of plastic deformation at the nanoscale level, that enhance the fracture toughness of nanocrystalline ceramics.

1. INTRODUCTION

Nanocrystalline ceramics (often called nanoceramics) represent ceramic materials consisting of at least one component with dimensions in the nanometer range (< 100 nm). Nanoceramics show outstanding mechanical and functional properties whose potential to transform so many technologies is really impressive. For instance, nanoceramics commonly have such technologically attractive characteristics as superior strength, superior hardness and good fatigue resistance [1–6]. At the same time, in most cases, superstrong nanoceramics at ambient temperatures show both low fracture toughness and poor ductility/machinability [3,7,8], which are undesired for practical applications. In particular, the low fracture toughness of nanocrystalline ceramics, as with conventional microcrystalline ceramics, is treated as the key factor limiting their practical utility [1].

Recently, certain progress has been achieved in enhancement of fracture toughness of ceramic nanocomposites at comparatively low homologous temperatures; see, e.g., reviews [1–5], book [6], and original papers [9–17]. (In addition, several research groups reported on enhanced ductility or even superplasticity of nanoceramics at comparatively low homologous temperatures [18–22].) These experimental data serve as a basis for the technologically motivated hopes to develop new superstrong nanocrystalline ceramics with good fracture toughness. To do so, of crucial interest are the specific micromechanisms responsible for enhancement of fracture toughness of nanoceramics. The main aim of this paper is to provide an overview of experimental studies, computer simulations and theoretical models focused on crack growth processes and micromechanisms for fracture toughness enhancement in nanoceramics.

2. SPECIFIC STRUCTURAL FEATURES OF NANOCERAMICS

The crack growth processes in nanoceramics strongly depend on their structural features and phase content. This section briefly describes the specific structural features of single-phase and composite nanoceramics.

Corresponding author: I.A. Ovid'ko, e-mail: ovidko@nano.ipme.ru

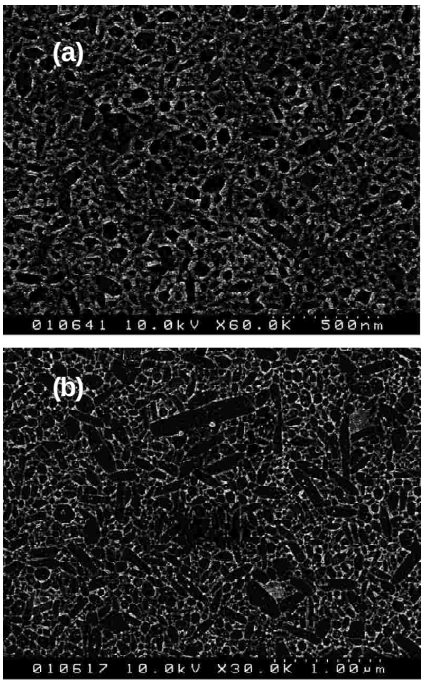

Fig. 1. Scanning electron microscopy photographs of Si_3N_4 nanoceramics. (a) The microstructure of as-received nanoceramics. (b) Nanoceramics after deformation at 1500 °C with a strain of 0.45 under initial strain rate of $3 \cdot 10^{-5}$ s^{-1}. Reprinted from [20]. Copyright 2006, with permission from Elsevier.

First, let us consider the structural features of single-phase nanocrystalline ceramics, compositionally homogeneous solids consisting of nanoscale grains (nanocrystallites) divided by grain boundaries (GBs) (Fig. 1). Their grains are specified by at least one size $d < 100$ nm and have a crystalline structure. In most cases, nanocrystalline ceramics consist of approximately equiaxed grains with a narrow grain size distribution (Fig. 1a). At the same time, there are other examples of grain geometry in nanocrystalline ceramics [20]. Besides, in recent years, nanocrystalline ceramics with a bimodal structure have been produced during superplastic forming [20]. The bimodal ceramic structure consists of both nanoscopic and microscopic rod-like grains (Fig. 1b). (Formation of such rod-like grains during superplastic deformation can effectively occur either by the Li mechanism of grain rotation resulting in coalescence of neighboring grains [23] or through stress-driven collective GB migration [24].)

The crystal lattices of grains are misoriented relative to each other. Neighboring grains are divided by GBs, flat or faceted layers that carry a geometric mismatch between adjacent misoriented crystalline grains (Fig. 1a). The typical thickness of conventional (non-amorphous) GBs is around 1 nm. Amorphous GBs have the thickness ranging from 1 to several nanometers. The atomic structure and properties of GBs are different from the structure and properties of grains. In particular, the arrangement of atoms in GBs is disordered compared to that in grain interiors. GBs join at triple junctions that are tubular regions with diameters around 1-2 nm when they adjoin conventional GBs (Fig. 1a). Triple junctions of conventional GBs are recognized as line defects, whose structure and properties are commonly different from those of GBs that they adjoin. Triple junctions of amorphous GBs are commonly amorphous and have typical diameter ranging from 1 to several nanometers. With the nanoscale range of grain sizes, both GBs and their triple junctions occupy large volume fractions in nanocrystalline ceramic materials and thereby strongly influence the mechanical properties of these materials.

In general, one can distinguish the following specific structural features of single-phase nanocrystalline ceramics, differentiating them from conventional coarse-grained polycrystalline ceramic materials:

(1) Grains have nanoscopic sizes. A typical grain size d does not exceed 100 nm.
(2) The volume fractions occupied by GBs and their triple junctions are large in nanocrystalline ceramics compared to those in coarse-grained polycrystals.
(3) GBs are short. GB length typically does not exceed 100 nm.

Now let us turn to the discussion of the specific structural features of composite nanocrystalline ceramics, compositionally inhomogeneous solids containing nanoscale grains (nanocrystallites) of at least one component phase. Typical composite nanocrystalline bulk structures are schematically presented in Fig. 2. They are as follows: a nanocrystalline composite consisting of approximately equiaxed nanoscale grains of different phases (Fig. 2a); a nanocrystalline composite consisting of grains of one phase, divided by GBs with a different chemical composition (second phase) (Fig. 2b); a nanocrystalline composite consisting of large grains of one phase, embedded into a nanocrystalline matrix of the second phase (Fig. 2c); a nanocrystalline composite consisting of large grains of one phase with nanoscale particles of the second phase located at GBs between large grains (Fig. 2d); a nanocrystalline composite

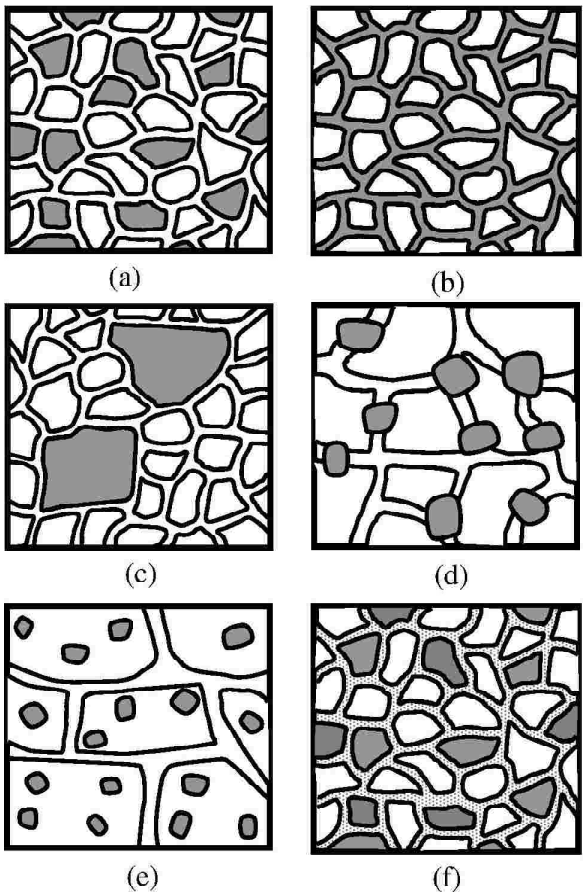

Fig. 2. Typical composite nanocrystalline bulk structures. (a) Nanocrystalline composite materials consisting of tentatively equiaxed nanoscale grains of different phases. (b) Nanocrystalline materials consisting of grains of one phase, divided by grain boundaries with different chemical composition (second phase). (c) Nanocrystalline composite materials consisting of large grains of one phase, embedded into a nanocrystalline matrix of the second phase. (d) Nanocrystalline composite materials consisting of large grains of one phase with nanoscale particles of the second phase located at grain boundaries between large grains. (e) Nanocrystalline composite materials consisting of nanocrystallites of one phase, embedded into the polycrystalline matrix of the second phase. (f) Nanocrystalline materials consisting of grains of two phases, divided by grain boundaries with different chemical composition (third phase).

consisting of nanocrystallites of one phase, embedded into the polycrystalline matrix of the second phase (Fig. 2e); a nanocrystalline composite consisting of grains of two phases, divided by GBs with a different chemical composition (third phase) (Fig. 2f). These and other typical classes of nanocomposite solids are discussed in detail by Niihara *et al.* [25] and Kuntz *et al.* [1].

It is difficult to identify the generic structural features of ceramic nanocomposites, because of their variety (Fig. 2). In most cases, however, GBs occupy large volume fractions in nanocomposites and thereby strongly affect the mechanical and other properties of these materials. GBs in nanocomposites often serve as interphase boundaries characterized by geometric or, in other words, phase mismatch between different crystalline lattices of different phases matched at these boundaries. In this situation, GBs carry both misorientation and phase mismatches between crystallites matched at these boundaries.

Note that nanoceramics are commonly fabricated at highly non-equilibrium conditions. Therefore, imperfections (voids, contaminations) typically exist in nanoceramics. Such fabrication-produced imperfections tend to be located at GBs and their triple junctions.

The special case is represented by amorphous GBs. Nanocrystalline ceramics, as with their microcrystalline counterparts, often contain amorphous GBs whose chemical composition can either coincide with or be different from that of nanocrystallites. The width of amorphous GBs ranges rather widely (from around one to several nanometers), depending on the chemical composition and fabrication conditions. Amorphous triple junctions in such nanoceramics are significantly extended compared to the triple junctions of conventional (non-amorphous) GBs in nanocrystalline ceramics. Nevertheless, in the nanoceramics with amorphous GBs, the crystalline phase commonly occupies the largest part of the volume fraction.

Thus, nanoceramics have specific structural features. As it will be discussed in the next sections, the structural features and phase content exert significant effects on fracture toughness of nanoceramics.

3. EXPERIMENTAL DATA ON FRACTURE TOUGHNESS OF NANOCERAMICS. TOUGHENING STRATEGIES WHICH DO NOT INVOLVE PLASTIC FLOW

In this section, we will discuss both the key experimental data concerning fracture toughness of nanoceramics and its improvement strategies which do not involve plastic flow. These experimental data and (experiment-based) strategies are as follows:

(i) Nanoceramics (with typical grain sizes d < 100 nm) and ultrafine-grained ceramics (with d < 500 nm) exhibit strength and toughness enhancement compared to their conventional microcrystalline counterparts; see, e.g., pioneering papers [25-27] and reviews [1–5]. In particular, ultrafine-grained and nanocrystalline ceramic composites could show the two to five times higher toughness and strength at room temperature than those of monolithic materials [1-5,25-27]. Also, it was pointed out that the hardness, toughness, strength and fracture resistance for creep and fatigue at high temperatures as well as the thermal shock fracture resistance were also strongly improved for ultrafine-grained and nanocrystalline composites [1-5,25-27]. The high values of strength of nanoceramics are treated to be related to the combined effects of several factors, such as reduction in flaw sizes (close to nanoscale grain sizes in nanocrystalline structures) and structural homogenization (leading to reduction of the residual stress level after sintering). Nanocomposite design gives a crucial impact into increase of strength of composite nanoceramics [1-5, 25-27].

(ii) Cracks in nanocrystalline ceramics with narrow grain size distributions tend to propagate along GBs. This statement is supported by the studies of fracture surfaces of such nanoceramics. For example, the fracture of TiN ceramics with nanoscale grains (with the size 18 nm) has an intergrain character [28]. At the same time, for nanoceramics containing both nanoscale (with the size around 80 nm) and microscale (with the size about 2 μm) grains, cracks propagate along the boundaries of smaller grains but penetrate the interior regions of larger grains [3,28]. Also, Pei *et al.* [15] studied TiC/a-C:H nanocomposite coatings that consist of 2–5 nm TiC nanocrystallites embedded in an amorphous hydrocarbon (a-C:H) matrix. They observed that microcracks induced by nanoindentation or sliding wear propagate along the column boundaries while the coatings without a columnar microstructure exhibit substantial toughness.

(iii) The mechanical properties and the fracture mode of nanoceramics in ceramic nanocomposites are dependent on the strength of GBs. Therefore, the mode of crack growth depends on the strength of different boundaries. For example, in Al_2O_3–SiC ceramic nanocomposites, the interfacial fracture energy between Al_2O_3 and SiC is twice that of the alumina GB fracture energy [29]. Besides, in such nanocomposites, the compressive stress generated by the SiC located within matrix grain may reinforce the Al_2O_3/Al_2O_3 GBs [17]. Therefore, the fracture toughness can be greatly improved, and the strong boundary may force the crack to deflect into the Al_2O_3 grain, thus forming the transgranular fracture mode, as it was observed by Liu *et al.* [17].

(iv) Nanoceramics can be toughened by means of the implantation of hard second-phase fibers that hinder crack propagation. When a propagating crack approaches a fiber, it can stretch, debond or fracture. In the latter two cases, the fiber is pulled out of the ceramic matrix. The deformation and/or fracture of the fiber require additional energy expenses for crack advance and thus increase fracture toughness. As an alternative, the crack approaching the fiber can change the direction of propagation and continue its advance along the fiber-matrix interface. This leads to crack deflection from its favorable orientation with respect to the direction(s) of the applied load and also results in increased fracture toughness [1].

Note that the fracture of a fiber in a ceramic nanocomposite as the result of crack propagation can be preceded by plastic deformation of the fiber. A theoretical analysis of such a mechanism of fiber fracture and pullout for the case of nanotube-reinforced ceramic nanocomposites, realized through the formation of circular dislocation loops around the nanotube, has recently been suggested [30]. It has been shown [30] that the generation and slip of circular prismatic dislocation loops along the fiber–matrix interface can be energetically favorable and barrier-less under a high but still realistic local shear stress acting in the interface near the crack surface.

Among various kinds of fibers, one can distinguish carbon nanotubes that have recently drawn much attention as reinforcing fibers due to their high strength (see, e.g., reviews [31,32] and original papers [9,16,33–45]). For example, Siegel *et al.* [16] observed the 24% increase in fracture toughness for a 10 vol.% multiwalled-carbon-nanotube (MWNT)–alumina composite, compared to that for the unfilled nanophase alumina (from 3.4 to 4.2 MPa $m^{1/2}$). Siegel *et al.* [16] observed that damage delocalization occurs as a result of well-dispersed nanotubes in the matrix.

Besides MWNTs, single-walled carbon nanotubes (SWNTs) have been used to reinforce nanocrystalline ceramics [9,37–45]. SWNTs are considered to be preferred for making composites, because the inner layers of MWNTs do not contribute considerably to carrying load, and therefore, for a given volume fraction of tubes, the stiffness of nanoceramic composites reinforced by MWNTs is lower than that of composites reinforced by SWNTs [46]. Moreover, the use of SWNTs as

reinforcing elements in the Al_2O_3 matrix has resulted in a dramatic increase in fracture toughness [9,39]. In particular, following Zhan *et al.* [9], the fracture toughness of the 5.7 vol.% SWNTs–Al_2O_3 nanocomposite (8.1 MPa $m^{1/2}$) is more than twice that of pure alumina (3.3 MPa $m^{1/2}$), and there is almost no decrease in hardness. Moreover, for 10 vol.% SWNT–Al_2O_3 nanocomposite, the toughness appeared to be as high as 9.7 MPa $m^{1/2}$, which is nearly three times that of pure Al_2O_3 sintered under identical conditions. The higher fracture toughness of SWNT-reinforced alumina nanoceramics compared to their MWNT-reinforced counterparts has been attributed primarily to the differences in the ability to transfer load from the matrix to the nanotubes. (The internal shells of MWNTs are unable to bond to the alumina matrix, and, therefore, tensile loads are carried entirely by the external shell [9].) Also, the high fracture toughness of SWNTs–Al_2O_3 nanocomposites can be associated with a unique entangling network structure of nanotubes, which leads to crack deflection along the continuous interface between carbon nanotubes and nanocrystalline alumina matrix grains [9].

At the same time, there is some controversy about the toughening in SWNTs–ceramics composites. For example, following Padture [32], the fracture toughness may depend on the test used to measure it. Most researchers use the simple indentation test to measure the toughness, which may not be valid for these composites (see Padture [32] and references therein). Other toughness tests (not based on indentation) show either no toughening [37], significant toughening [41] (two-fold increase over unreinforced ceramic) or unclear results [45].

Recently, Padture [32] has assumed that a high increase in fracture toughness observed in some experiments with SWNTs–ceramics composites is due to the action of a specific toughening mechanism, namely uncoiling and stretching of SWNTs. This mechanism is based on two peculiarities of SWNTs–ceramics composites. The first peculiarity is that the ends of SWNTs are located at GBs, which serve as anchors for SWNTs. The second specific feature of such composites lies in the fact that SWNTs, which are highly flexible, are commonly rolled, forming complicated tangles. As a result, when an advancing crack approaches a conventional rigid bridging fiber, the latter stretches or detaches from the matrix. At the same time, if a crack approaches SWNTs, the latter can uncoil (or unfurl) in the crack wake. With further propagation of the crack, the uncoiled SWNTs stretch, and eventually the SWNT bridges far behind the crack tip pullout or detach from the GBs and/or fail [32].

Along with the toughening by means of the implantation of hard fibers, nanoceramics can be dramatically toughened through a phase transformation [1,18,47–50]. This concerns ceramics containing zirconia. Transformation-induced toughening is based on the transformation of zirconia from the tetragonal to the monoclinic phase. This transformation occurs under an applied stress concentrated near a crack tip and should be stabilized by a dopant (yttria or yttria-based composite). The transformation creates inelastic strain that locally relieves the stress field near the crack tip and thus significantly increases fracture toughness. The effect of transformation in zirconia on fracture toughness strongly depends on the zirconia grain size [48,51]. Besides the use as a major phase of ceramics, nanocrystalline zirconia is exploited as a toughening agent in alumina-based nanoceramics [51].

Also, Choi *et al.* [52] and Choi and Awaji [53] suggested a qualitative description/strategy for modest enhancement of fracture toughness in composite nanoceramics consisting of polycrystalline matrix with embedded nanoparticles located at GBs and/or in grain interiors (Figs. 2d and 2e). Within this approach, during fabrication of such composite nanoceramics, the misfit stresses between the matrix and dispersed particles create misfit dislocations at interphase boundaries between the nanoparticles and the matrix. When temperature decreases, misfit dislocations move into grain interiors of the matrix. Propagation of a crack through the dislocated matrix initiates generation of nanocracks at these dislocations serving as stress sources. As a result of multiple generation of nanocracks in the vicinity of a crack tip, elastic energy in part releases, and crack growth is hampered [52,53].

Thus, as it has been shown in experiments, fracture toughness of nanoceramics is sensitive to their structure and nanocomposite design. There are several approaches (which do not involve plastic flow and are based on experiments) to enhancement of fracture toughness of ceramic nanocomposites at comparatively low homologous temperatures. These include conventional approaches typical of ceramics with various grain sizes (e.g., toughening by hard fibers, toughening by phase transformations) as well as strategies exploiting the specific nanostructural features (e.g., toughening by carbon nanotubes, toughening due to effects of misfit dislocations generated at nanoparticle/matrix interfaces).

4. TOUGHENING MECHANISMS ASSOCIATED WITH NANOSCALE PLASTIC DEFORMATION IN NANOCERAMICS: THEORETICAL MODELS AND COMPUTER SIMULATIONS

4.1. Toughening mechanisms associated with plastic flow in nanoceramics. General aspects

Along with the toughening mechanisms related to either the composite structure of nanoceramics or phase transformations, fracture toughness of nanoceramics can be enhanced due to the mechanisms associated with nanoscale plastic deformation. In general, plastic deformation in nanoceramics has its specific peculiarities due to the specific structural features of nanoceramics, differentiating them from conventional microcrystalline ceramics. With the specific peculiarities of plastic deformation in nanoceramics, several specific toughening micromechanisms/strategies have been proposed. The specific toughening micromechanisms/strategies involve nanoscale plastic flow as the crucial factor effectively hampering crack growth. The toughening micromechanisms/strategies related to nanoscale plastic flow are typically based on theoretical models and computer simulations of crack growth. In this section, we will discuss the key toughening micromechanisms/strategies associated with nanoscale plastic flow in nanoceramics.

It is well known that lattice dislocation slip – the dominant mode of plastic flow in metals – is suppressed in ceramics at ambient temperatures. The suppression is dictated by a high Peierls barrier for lattice dislocation slip. (A high Peierls barrier in ceramics is attributed to narrow cores of dislocations as well as to ionic and covalent interatomic bonds [54].) Nevertheless, lattice dislocation slip effectively operates in conventional microcrystalline ceramics at high homologous temperatures (exceeding temperature $\approx 0.5T_m$, where T_m is the melting temperature). At the same time, lattice dislocation slip is hampered or even suppressed in nanocrystalline ceramics, even at high homologous temperatures.

In nanocrystalline ceramic materials, as well as in nanocrystalline metals, the role of lattice dislocation slip is diminished due to nanoscale and interface effects. At the same time, in these materials alternative deformation modes mediated by grain and interphase boundaries come into play [2,3,8,55–66]. In particular, such alternative deformation modes represent GB sliding, GB diffusional creep (Coble creep), triple junction diffusional creep and rotational deformation mode in nanocrystalline materials [2,3,57–66].

For instance, the first stage of plastic deformation in nanoceramics predominantly occurs in the interfacial phase [56,67]. With an increase in the applied stress level, both intergranular and intragranular deformation processes occur in nanocrystalline SiC [67]. In this event, intragranular deformation is realized through emission of lattice dislocations from the interfacial phase, their slip in nanoscale grains and absorption at interfaces [67]. (This process is very similar to plastic flow involving emission of lattice dislocations from either low- or high-angle GBs in nanocrystalline metals [58,68,69]. The active role of the specific (alternative) deformation modes in plastic flow in nanoceramic materials is capable of causing specific toughening mechanisms in these materials.

Let us consider the effects of plastic deformation in nanoceramics on their fracture toughness. In general, one expects conventional and new toughening mechanisms to operate in nanocrystalline single-phase and composite ceramics. For instance, as with their microcrystalline counterparts, nanoceramics can be toughened by means of the implantation of inclusions of a ductile (metallic) phase. Following Kuntz *et al*. [1], the ductile phase can lead to the toughening of the composite either through ductile yielding in the region of a propagating crack or by ductile bridging ligaments in the crack wake. In the first case, crack propagation is hindered due to the plastic deformation of the ductile phase or blunting of the crack tip at a ductile particle. In the second case, crack propagation is retarded by ductile bridging ligaments in the crack wake. This occurs when the crack tip propagates past a ductile-phase grain that then bridges the crack wake and must be pulled to failure or debonds from the surrounding matrix. Note that the conventional toughening mechanisms – ductile phase toughening, fiber toughening and transformation toughening – have their analogs operating in microcrystalline ceramics [1]. At the same time, the action of these conventional mechanisms in nanoceramics has its specific features due to the specific structural features (first of all, the presence of nanoscale crystallites and a large amount of the interfacial phase) of the nanoceramics.

In addition to the conventional mechanisms, special (new) toughening mechanisms are expected

to effectively operate in nanoceramics due to the nanoscale and interface effects. In particular, strong candidates for such special mechanisms are the toughening by interface-mediated plastic deformation, the toughening by local lattice rotation in nanoscale crystallites, the toughening by stress-driven GB migration, and the toughening by enhanced interfacial diffusion. The special toughening mechanisms in nanoceramics should be controlled by the nanoscale plastic flow processes. These processes result in nanoscale structural inhomogeneities releasing, in part, the stresses near the propagating crack tip. In particular, such plastic flow processes as intense interfacial sliding and Coble creep carried by interfacial defects as well as transformations of such defects (e.g., nucleation and climb of interfacial dislocations) create nanoscale defect configurations whose stress fields, in part, accommodate the stresses near the propagating crack tip. Also, nanoscale rotational deformation and stress-driven GB migration create nanoscale configurations of disclinations (defects of the rotational type) causing a similar stress relaxation near the propagating crack. All these nanoscale plastic relaxation mechanisms enhance the toughening behavior of ceramic nanocomposites and are not typical in microcrystalline ceramics.

4.2. Toughening mechanism associated with grain boundary deformation processes. Phenomenological approach

Recently, Pozdnyakov and Glezer [70] have theoretically examined the fracture toughness of a quasi-brittle nanomaterial, where GB deformation occurs and a large crack propagates through the consecutive generation of nanocracks near its tip. The GB deformation has been accounted for by the introduction of a strengthening coefficient, and the nanocrack near the tip of a large propagating crack has been assumed to form if the local stress exceeds a critical value. As a result, Pozdnyakov and Glezer [69] concluded that plastic deformation carried by GBs can significantly increase the fracture toughness of nanocrystalline ceramics. However, the exact value of fracture toughness depends on the strengthening coefficient (which is, in turn, determined by plastic deformation modes operating near the crack tip) and cannot be found within this approach.

Along with the examination of the step-by-step crack growth along GBs, Pozdnyakov and Glezer [70] theoretically analyzed the propagation of cracks through the regions occupied by grain interiors, GBs and triple junctions of GBs in nanocrystalline metals and ceramics. They indicated that the fracture toughness depends on the volume fractions of grain interiors, GBs and triple junctions. Also, they assumed that the critical energy release rate can be averaged over the volume of the three phases (grain interiors, GBs and triple junctions) to obtain the fracture toughness.

4.3. Toughening mechanism associated with interactions between lattice dislocations and grain boundaries. Computer simulations

Now let us consider computer simulations of fracture toughness enhancement due to plastic flow in nanocrystalline materials. Shimokawa *et al.* [71] has performed molecular dynamics simulations of an aluminum bicrystal containing a crack and <112> tilt grain boundaries. They aimed to explain the results of experiments [72,73] concerning an increase in fracture toughness of ultrafine-grained iron compared to that of coarse-grained iron. Although their study was focused on ultrafine-grained metals, their results can possibly be extended to the case of ultrafine-grained ceramics deformed at elevated temperatures at which dislocation motion in ceramics is possible. The same is valid for some of the computer and theoretical models that will be discussed below, because they are effective in description of crack growth in both ceramics and metals having nanocrystalline structures.

Based on the results of molecular dynamics simulations, Shimokawa *et al.* [71] proposed the following scenario of deformation of ultrafine-grained metals near crack tips. At the beginning of the deformation, a crack tip acts as the main dislocation source and can generate dislocations. These dislocations produce pile-ups, and the leading dislocations of these pile-ups stop at the nearby GBs. The dislocations emitted from the crack tips reduce stress concentration at the crack tip (that is, shield the crack), thereby hampering its growth. As a result, the fracture toughness of a solid becomes larger than it would be in the case of purely brittle fracture (without dislocation emission from the crack tip). However, the stress intensity factor required for dislocation emission from the crack tip also increases with the number of dislocations around the crack tip, and then it becomes difficult to make further emission of dislocations from the crack tip. Since the number of dislocations emitted

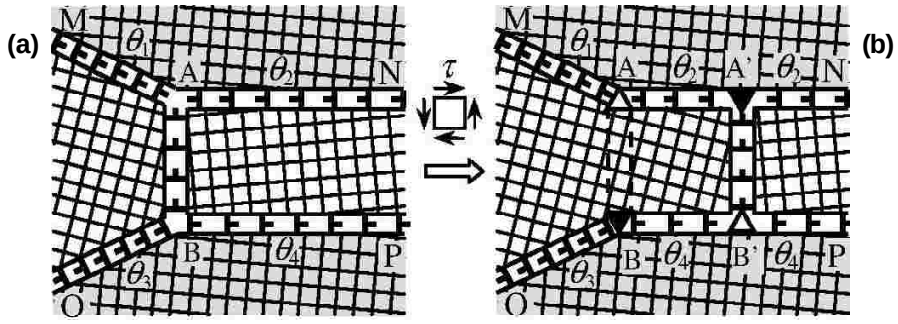

Fig. 3. Stress-induced migration of a tilt boundary in a nanocrystalline specimen (two-dimensional model). The vertical tilt boundary migrates from its initial position AB (a) to the final position A'B' (b). The shear coupled to migration is accommodated by formation of disclinations (triangles) at grain boundary junctions A, A', B, and B'. Reprinted from [77]. Copyright 2008, with permission from Elsevier.

from the crack tip (as well as their shielding effect) decrease with decreasing grain size, fracture toughness should become small as the grain size becomes small. This result within similar models of dislocation emission from crack tips has also been obtained previously in analytical models [74,75]. At the same time, the molecular dynamics simulations performed in Ref. [71] demonstrated that stress concentration produced by the crack and dislocation pile-ups as well as the formation of non-equilibrium (extrinsic) dislocations in GBs due to dislocation emission from the crack tip can initiate multiple dislocation emissions from GBs near the crack tip. Dislocation emissions from unstable GBs are accompanied by transformation of GB structure into the neighboring favored boundary and results in the formation of an uncompensated dislocation charge at GBs. The results of molecular dynamics simulation show that the uncompensated dislocation charge at GBs is equivalent to that created by a dipole of GB disclinations. When the dislocations emitted from GBs have the character of an antishielding effect on the crack tip, the disclination dipole necessarily induces a shielding effect on the crack tip. Disclination shielding can be activated when a transition of dislocation sources from crack tips to GBs occurs, and the effect becomes pronounced as anti-shielding dislocations are continuously emitted from GBs without dislocation emissions from crack tips. This mechanism can shield the stress field around the crack tip and lead to plastic deformation by dislocation emissions from GBs; hence it can be expected that the disclination shielding effect can improve the fracture toughness in ultrafine-grained and nanocrystalline solids.

Sangid *et al.* [76] have studied the effect of GBs on fatigue crack growth in a nanocrystalline NiCo alloy. They aimed to explain a good resistance of this alloy to fatigue crack propagation. They suggested that one of the reasons for a good resistance to fatigue crack growth is associated with the nanocrystalline structure of the alloy. According to their model, there is competition between dislocation emission from the crack tip and crack advancement. They considered the situation where the fatigue crack propagates through the consecutive steps of dislocation emission and crack blunting during the forward loading and crack sharpening and dislocation emission along another slip plane during the reverse loading. In a nanocrystalline solid, in spirit of the approach [74,75], the nearby GBs can act as stoppers for dislocations and hamper considerable dislocation emission from crack tips, thus retarding fatigue crack propagation.

4.4. Stress-driven migration of grain boundaries as a toughening mechanism

Now let us consider the effect of stress-driven migration of GBs on fracture toughness of nanoceramics [77,78]. The stress-driven GB migration is treated as a special deformation mode operating in nanocrystalline materials [79,80]. The stress-driven migration creates GB disclinations (line defects dividing GB fragments with different misorientation parameters [81,82]), and the disclination stress fields hamper crack growth [79,80]. Following [79], let us discuss the geometry of the stress-induced GB migration and its accommodation in nanocrystalline ceramics. In doing so, in order to simplify our analysis, we consider a two-dimensional model arrangement of nanoscale grains with pure tilt GBs, including a vertical GB that migrates in a rectangular grain as shown in Fig. 3. The tilt GBs are either low- or high-

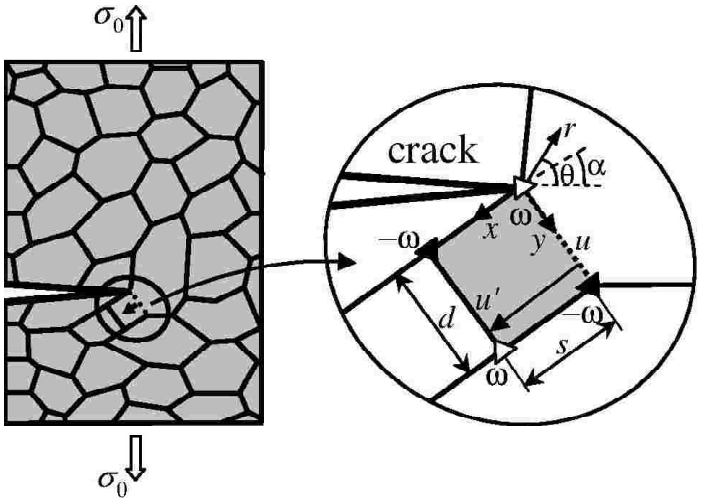

Fig. 4. Grain boundary migration and formation of a disclination quadrupole in a deformed nanoceramic solid. Reproduced from [78], with permission.

angle boundaries containing discrete or continuously distributed dislocations, as schematically shown in Fig. 3. In particular, the vertical GB contains a finite-wall-like ensemble of dislocations that provide its tilt misorientation ω. In its initial state, the vertical GB (Fig. 3a) terminates at the GB junctions A and B, which are supposed to be geometrically compensated. There are no angle gaps at these triple junctions or, in other words, the sum of tilt misorientation angles of all GBs joining at each of these junctions is equal to zero, where summation of the angles is performed clockwise along a circuit surrounding a triple junction [83, 84].

In the case under consideration, the following balance equations are valid:

$$\theta_1 + \theta_2 = -\omega \text{ (for GB junction A)}, \quad (1)$$

$$\theta_3 + \theta_4 = \omega \text{ (for GB junction B)}. \quad (2)$$

Following the geometric theory of triple junctions [83,84], the geometrically compensated GB junctions A and B (Fig. 3a) do not create long-range stresses.

Let us consider the situation where the vertical GB migrates from the position AB to the position A'B' (Fig. 3b), and no other accommodating structural transformations occur. As a result of the migration, the angle gaps $-\omega$ and ω appear at the GB junctions A and B, respectively [79] (Fig. 3b). That is, the sum of the misorientation angles at the junction A after GB migration is $\theta_1 + \theta_2$, which is equal to $-\omega$ according to formula (1). The sum of the misorientation angles at the junction B after GB migration is $\theta_3 + \theta_4$, which is equal to ω according to formula (2). Also, GB migration results in the formation of two new triple junctions A' and B' characterized by the angle gaps ω and $-\omega$, respectively. That is, the sum of the misorientation angles at the junction A' is equal to ω, as it is directly seen in Fig. 3b. The sum of the misorientation angles at the junction B' is equal to $-\omega$ (Fig. 3b).

Within the theory of defects in solids, the GB junctions A, B, A', and B' characterized by the angle gaps $\pm\omega$ are defined as partial wedge disclinations that serve as powerful stress sources characterized by the disclination strengths $\pm\omega$ [60, 82–86]. The disclinations at the points A, B, A', and B' form a quadrupole configuration whose formation accommodates GB migration coupled to shear in a nanocrystalline specimen. The disclination quadrupole creates internal stresses screened at distances being around the largest size (largest interspacing between the disclinations) of the quadrupole.

Morozov *et al.* [78] have calculated the effect of GB migration near the tip of a pre-existent crack on the fracture toughness of nanocrystalline ceramics. They considered migration of a GB near the tip of a mode I crack in a nanocrystalline ceramic solid (Fig. 4). Within the model [78], the crack has a length l and occupies the region ($-l < x < 0$, $y = 0$), while the crack tip $x = y = 0$ lies in a junction of two GBs. One of these GBs of length d, denoted as u (Fig. 4), is supposed to make an angle $\alpha - \pi$ with the x-axis and the right angle with the neighboring GB. Due to the action of a tensile applied load and its concentration near the crack tip GB u migrates by a distance s to a new position u' (Fig. 4). GB migration results in the formation of a disclination

quadrupole, which shields the crack tip and thereby increases fracture toughness.

Following [78], let us consider the effect of the disclination quadrupole formed due to GB migration on the fracture toughness of the nanocrystalline solid. Within the approach [78], the nanocrystalline solid was modeled as an elastically isotropic medium with the shear modulus G and Poisson's ratio ν. In calculation of the fracture toughness of the nanocrystalline solid, the authors of [78] used the crack growth criterion [87] based on the balance between the driving force related to a decrease in the elastic energy and the hampering force related to the formation of new free surfaces during crack growth. In the examined case of the plane strain state, this criterion has the form [87]:

$$\frac{1-\nu}{2\mu}\left(K_I^2 + K_{II}^2\right) = 2\gamma_e, \tag{3}$$

where K_I and K_{II} are the intensity factors for normal (to crack line) and shear stresses, respectively; and γ_e is the effective specific surface energy. Here $\gamma_e = \gamma$ (where γ is the specific surface energy) for the crack propagating inside a grain, and $\gamma_e = \gamma - \gamma_b/2$ (where γ_b is the specific GB energy) for the crack that advances along a GB. In the considered situation where the crack growth direction is perpendicular to the direction of the external load, the coefficients K_I and K_{II} are given as:

$$K_I = K_I^\sigma + k_I^q, \quad K_{II} = k_{II}^q. \tag{4}$$

Here K_I^σ is the stress intensity factor induced by the applied load σ_0, while k_I^q and k_{II}^q are the intensity factors for the stresses created by the disclination quadrupole located near the crack tip (Fig. 4).

Within the macroscopic mechanical description, the effect of the local plastic flow – the special rotational deformation resulting in the formation of a disclination quadrupole – on crack growth can be accounted for through the introduction of the critical stress intensity factor K_{IC}. In this case, the crack is considered as propagating under the action of the tensile load perpendicular to the crack growth direction, while the presence of the disclination quadrupole simply changes the value of K_{IC} compared to the case of brittle crack propagation. In these circumstances, the critical condition for the crack growth can be represented as (see, e.g., [88]): $K_I^\sigma = K_{IC}$.

With expressions (2) substituted to formula (1) and the critical condition $K_I^\sigma = K_{IC}$ taken into account, one finds the following expression for K_{IC}:

$$K_{\mathrm{IC}} = \sqrt{\left(K_{\mathrm{IC}}^\sigma\right)^2 - \left(k_{\mathrm{IIC}}^q\right)^2} - k_{\mathrm{IC}}^q. \tag{5}$$

In formula (5) $K_{IC}^\sigma = \sqrt{4G\gamma_e/(1-\nu)}$ is the fracture toughness in the disclination-free case (that is, in the case of brittle fracture with the special rotational deformation being completely suppressed), $k_{IIC}^q = k_{II}^q\big|_{K_I^\sigma = K_{IC}}$ and $k_{IC}^q = k_I^q\big|_{K_I^\sigma = K_{IC}}$. In order to characterize the effect of the disclination quadrupole produced by the special rotational deformation (Fig. 4) on crack growth, one should compare the critical stress intensity factor K_{IC} with the quantity K_{IC}^σ.

Following [78], let us consider the critical stress intensity factor K_{IC} in the situation where the disclination quadrupole forms near the crack, as shown in Fig. 4. Along with the Cartesian coordinate system (x,y) one introduces a polar coordinate system (r, θ) with the origin at the crack tip (see Fig. 4). The quadrupole arms are assumed to be small compared to the crack length l (s,d << l). This assumption allows one to model the crack as a semi-infinite crack in the calculation of the stress intensity factors k_I^q and k_{II}^q. (In the limit of a semi-infinite crack, the disclination ω at the crack tip becomes located at an external free surface and disappears, in which case the disclination quadrupole transforms into three disclinations.) The stress intensity factors k_I^q and k_{II}^q for the disclination quadrupole shown in Fig. 4 are given as follows [78]:

$$k_I^q = G\omega\sqrt{d}\,f_1(\alpha,t)/\left[2\sqrt{2\pi}\left(1-\nu\right)\right],$$

$$k_{II}^q = G\omega\sqrt{d}\,f_2(\alpha,t)/\left[2\sqrt{2\pi}\left(1-\nu\right)\right],$$

where $t = s/d$,

$$f_1(\alpha,t) = \sum_{k=1}^{3}(-1)^k\sqrt{\tilde{r}_k}\left[3\cos\left(\theta_k/2\right) + \cos\left(3\theta_k/2\right)\right], \tag{6}$$

$$f_2(\alpha,t) = \sum_{k=1}^{3}(-1)^k\sqrt{\tilde{r}_k}\left[3\sin\left(\theta_k/2\right) + \sin\left(3\theta_k/2\right)\right],$$

$\tilde{r}_k = r_k/d$, and r_k and θ_k are the coordinates of the kth disclination (k = 1,2,3) and $-\pi < \theta_k \le \pi$. For the disclination quadrupole shown in Fig. 4 and α in the range $-\pi < \alpha \le \pi$, we have: $\tilde{r}_1 = 1$, $\tilde{r}_2 = \sqrt{t^2+1}$, $\tilde{r}_3 = t$; $\theta_1 = \alpha$, $\theta_2 = \alpha - \pi/2 + \mathrm{arccot}\,t + 2\pi\Xi(-\alpha - \pi/2 - \mathrm{arccot}\,t)$, $\theta_3 = \alpha - \pi/2 + 2\pi\Xi(-\pi/2 - \alpha)$, $\Xi(x)$ is the Heaviside function equal to unity for $x > 0$ and zero otherwise.

The equilibrium value of the GB migration length should correspond to a minimum of the ΔW

associated with the formation of the disclination quadrupole (Fig. 4). The energy change ΔW has been calculated in [78]. In the calculation, the weak effect of the crack on the disclination quadrupole self-energy was neglected while the influence of the crack on the interaction of the quadrupole with the stress field due to the applied tensile load was rigorously taken into account. As a result, Morozov *et al.* [78] obtained the following expression for the energy change ΔW:

$$\Delta W = D\omega^2 d^2 h(t)/2 - K_I^{\sigma}\omega d^{3/2} f(\alpha,t)/\left(3\sqrt{2\pi}\right), \tag{7}$$

where $D = G/[2\pi(1-\nu)]$, $t = s/d$, as above,

$$h(t) = (1+t^2)\ln(1+t^2) - t^2\ln(t^2), \tag{8}$$

$$f(\alpha,t) = \begin{cases} g_1(\theta,\alpha)\big|_{\theta=\operatorname{arccot} t}^{\pi/2} + t^{3/2} g_2(\theta,\alpha)\big|_{\theta=0}^{\operatorname{arccot} t}, & -\pi/2 < \alpha \le \pi, \\ g_1(\theta,\alpha)\big|_{\theta=\operatorname{arccot} t}^{\alpha+\pi/2} - g_1(\theta,\alpha)\big|_{\theta=\alpha+\pi/2}^{\pi/2} + t^{3/2} g_2(\theta,\alpha)\big|_{\theta=0}^{\operatorname{arccot} t}, & -\pi < \alpha \le -\pi/2 - \operatorname{arccot} t, \\ -g_1(\theta,\alpha)\big|_{\theta=\operatorname{arccot} t}^{\pi/2} + t^{3/2}\left(g_2(\theta,\alpha)\big|_{\theta=0}^{\alpha+\pi/2} - g_2(\theta,\alpha)\big|_{\theta=\alpha+\pi/2}^{\operatorname{arccot} t}\right), & -\pi/2 - \operatorname{arccot} t < \alpha \le -\pi/2, \end{cases} \tag{9}$$

$$g_1(\theta,\alpha) = \frac{4\sin^2\left[\left(\theta+\alpha+\pi/2\right)/2\right]\cos\left[\left(\theta-\alpha-\pi/2\right)/2\right]}{\sqrt{\sin\theta}}, \tag{10}$$

$$g_2(\theta,\alpha) = \frac{4\sin^2\left[\left(\theta+\alpha+\pi/2\right)/2\right]\sin\left[\left(\theta-\alpha-\pi/2\right)/2\right]}{\sqrt{\cos\theta}}. \tag{11}$$

GB migration is possible if $\partial\Delta W/\partial s\big|_{s\to 0} \le 0$. Substituting formulae (7)–(11) to the latter relation, one obtains that at $\omega > 0$, GB migration in the direction shown in Fig. 4 is possible. In the case $0 \le \alpha \le \pi$, GB migration also takes place but in the opposite direction.

The equilibrium length s_0 of GB migration, if it exists, follows from the relation $\partial\Delta W/\partial s\big|_{s\to s_0} = 0$ and formulae (7) and (8). The equation for s_0 has the form

$$G\omega\sqrt{d} = \left.\frac{\sqrt{2\pi}\left(1-\nu\right)K_I^{\sigma}\partial f(\alpha,t)/\partial t}{3t\ln(1+1/t^2)}\right|_{t=t_0}, \tag{12}$$

where $t_0 = s_0/d$.

Now let us calculate the stress intensity factors k_I^q and k_{II}^q for the case where the equilibrium length of GB migration (characterized by the equality $t = t_0$) exists. Substituting the latter equality and formula (12) to the expressions for k_I^q and k_{II}^q, one obtains $k_I^q = AK_I^{\sigma}$, $k_{II}^q = BK_I^{\sigma}$, where

$$A = \left.\frac{f_1(\alpha,t)\partial f(\alpha,t)/\partial t}{6t\ln(1+1/t^2)}\right|_{t=t_0}, \quad B = \left.\frac{f_2(\alpha,t)\partial f(\alpha,t)/\partial t}{6t\ln(1+1/t^2)}\right|_{t=t_0}. \tag{13}$$

Insertion of the latter relations for k_I^q and k_{II}^q to formula (5) and solving the resulting equation for K_{IC} yields

$$K_{IC} = \frac{K_{IC}^{\sigma}}{\sqrt{\left(1+A\right)^2 + B^2}}. \tag{14}$$

As follows from formula (14), GB migration increases the value of K_{IC} (that is, provides fulfillment of the condition $K_{IC} > K_{IC}^{\sigma}$) if $-2 < A < 0$ and $|B| < \sqrt{-A\left(A+2\right)}$. Besides, from formula (13) it follows that the quantities A and B depend on the parameters α and t_0 only. As a consequence, the normalized critical stress intensity factor K_{IC}/K_{IC}^{σ} (calculated using formula (14)) also depends on α and t_0 only. In turn, the parameter t_0 can be related to the disclination strength ω and material parameters. For this purpose, consider a critical crack (characterized by the equality $K_{IC} = K_{IC}^{\sigma}$) and substitute this equality, formula (14) and the relation $K_{IC}^{\sigma} = \sqrt{4G\gamma_e/\left(1-\nu\right)}$ to formula (12). Then one finds:

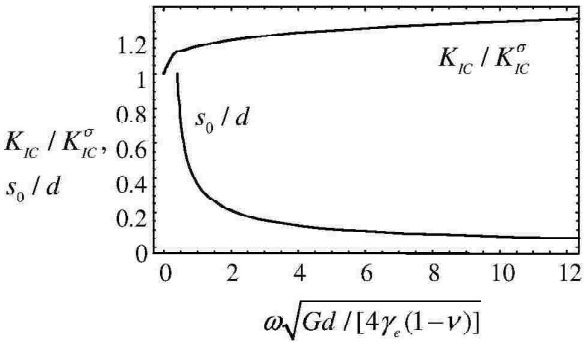

Fig. 5. Dependences of the normalized fracture toughness K_{IC}/K_{IC}^{σ} and normalized migration length s_0/d on the parameter $\omega\sqrt{Gd/\left[4\gamma_e\left(1-\nu\right)\right]}$, that characterizes the disclination strength ω, for $\alpha = \pi/6$.

$$\omega\sqrt{\frac{Gd}{4\gamma_e\left(1-\nu\right)}} = \left.\frac{\sqrt{2\pi}\,\partial f(\alpha,t)/\partial t}{3\sqrt{\left(1+A\right)^2+B^2}\;t\ln\left(1+1/t^2\right)}\right|_{t=t_0}. \qquad (15)$$

The dependences of the normalized critical stress intensity factor K_{IC}/K_{IC}^{σ} and normalized equilibrium migration length s_0/d on the parameter $\omega\sqrt{Gd/\left[4\gamma_e\left(1-\nu\right)\right]}$, calculated using formulae (14) and (15), are shown in Fig. 5 for the case $\alpha = \pi/6$. As follows from Fig. 5, for a GB of specified length d, the equilibrium GB length s_0 decreases with an increase in ω, while the critical stress intensity factor K_{IC} increases with ω. At small enough ω the equilibrium GB length tends to infinity. In this case, GB migration should in reality be restricted only by the presence of neighboring GBs.

Following [78], assume that fracture in the examined nanocrystalline solid occurs through multiple crack propagation, which is affected by the formation of numerous disclination quadrupoles near crack tips. Taking into account the short-range character of the stress field of disclination quadrupoles, Morozov *et al.* [78] also supposed that crack propagation is affected only by the migration of the GB adjacent to the crack tip. Besides, for simplicity, Morozov *et al.* [78] neglected the distribution of GBs over misorientation angles and put the misorientations of all GBs equal to ω.

In this case, as a first approximation, the fracture toughness of the nanocrystalline solid can be defined as the average value of K_{IC} over various values of the angle α. For simplicity, following [78], suppose that only one GB migrates near the tip of any crack (migration of two or more GBs will, apparently, increase fracture toughness). Assuming that the angle α is random, we introduce a distribution in α described by the distribution function $\rho_\alpha(\alpha) = 1/(2\pi)$, $-\pi < \alpha \le \pi$. Taking into account that $K_{IC}(\alpha,\omega) = K_{IC}(-\alpha,\omega)$ [78], the fracture toughness $\overline{K_{IC}}$ can be calculated as

$$\overline{K_{IC}}(\omega) = \left(1/\pi\right)\int_0^{\pi} K_{IC}(\alpha,\omega)\,\mathrm{d}\alpha. \qquad (16)$$

Using formula (16), let us calculate the fracture toughness for the case of nanocrystalline ceramic 3*C*-SiC with the following parameter values: $G = 217$ GPa, $\nu = 0.23$, $\gamma = 1.84$ [78] and $d = 15$ nm. Then for the case of an intragrain crack and $d = 15$ nm, one has $\overline{K_{IC}}/K_{IC}^{\sigma} \approx 1.133$, 1.108, and 1.102, for $\omega = 5°$, 15°, and 30°, respectively. For the case of an intragrain crack and $d = 30$ nm, we have: $\overline{K_{IC}}/K_{IC}^{\sigma} \approx 1.124$, 1.104, and 1.102 , for $\omega = 5°$, 15°, and 30°, respectively. As follows from these data, weakly increases with a decrease in GB misorientation angle ω and/or grain size d. In general, in 3*C*-SiC GB migration can increase fracture toughness by 10-15%.

4.5. Nanoscale twin deformation and Ashby-Verall creep as toughening mechanisms

Recently, nanoscale twin deformation carried by partials emitted from GBs has been theoretically shown to be a specific toughening mechanism in nanocrystalline ceramics and metals [90]. The model [90] describes the generation of deformation twins near cracks of mixed I and II modes in nanocrystalline metals and ceramics. In the framework of the model, a deformation twin nucleates through stress-driven emission of twinning dislocations from a GB distant from the crack tip. The deformation twin nucleation releases, in part, high local stresses near the crack tip and thereby enhances fracture toughness.

Also, creep deformation conducted by GB processes (Ashby-Verall creep carried by intergrain sliding accommodated by GB diffusion and grain rotations [91,92]) has been suggested as a toughening mechanism inherent to nanocrystalline metals [93,94]. Although the focus of Refs. [93] and [94] is on nanocrystalline metals, their approach can be extended to the situation with nanoceramics. At the same time, the creep deformation considered

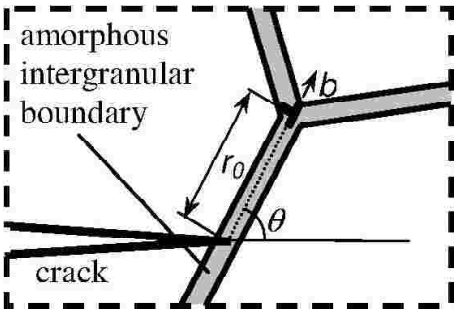

Fig. 6. Edge dislocation at the amorphous intergranular boundary near the tip of a long crack that intersects the boundary. Reproduced from [95], with permission.

in these references is a slow diffusion-controlled process which can effectively contribute to toughening of nanocrystalline materials only in the limiting partial cases where diffusion is very fast (at high temperatures) and/or crack growth is extremely slow.

4.6. Grain boundary sliding as a toughening mechanism

Nevertheless, there are expectations that GB sliding can effectively contribute to toughening of nanocrystalline materials in a more general situation with comparatively wide ranges of crack tip velocity and temperature. For instance, let us consider the specific toughening mechanism associated with GB sliding in nanoceramics with amorphous GBs [95]. It is known that the mechanical behavior of nanocrystalline ceramics is strongly influenced by GB deformation processes in amorphous GBs often existing in such materials; see, e.g., experimental data [1,20–22] and computer simulations [67,96]. For instance, following experimental data on Si_3N_4-based ceramics and ceramic composites, compressive creep in these materials takes place through GB sliding [97–102]. Also, following computer simulations [67,96] of the evolution of the nanocrystalline cubic phase of silicon carbide (3C-SiC) under a mechanical load, plastic deformation intensively occurs within amorphous GBs in these nanocrystalline ceramics.

Bobylev *et al.* [95,103] have studied the effect of GB sliding on crack growth in nanocrystalline ceramics. They assumed that GB sliding is not accommodated at low temperatures and is accommodated at high enough temperatures. Following [95,103], first, consider the situation where the solid is strained at a sufficiently low temperature ($T<T_{GBD}$), where $T_{GBD} \approx 0.3T_m$ is the temperature of activation GB diffusion and T_m is the melting temperature. In this case cracks initiate GB sliding which leads to generation of immobile dislocations at triple junctions of GBs. The GB-sliding-produced dislocations cause partial stress relaxation in the vicinities of crack tips and thereby hamper crack growth. A dislocation (Fig. 6) is generated due to GB sliding along an amorphous GB in a nanocrystalline ceramic specimen. The Burgers vector magnitude of the dislocation at the boundary gradually grows [95] (because of GB sliding arrested at the triple junction) in parallel with local plastic strain carried by GB sliding in this boundary. The direction of the dislocation Burgers vector is parallel to the boundary line (plane in the three-dimensional case). The examined dislocations are treated in terms of the Volterra theory of dislocations in continuum media [104,105] as dislocation-like sources of internal stresses (but not conventional lattice dislocations). Such dislocations are commonly immobile at triple junctions of amorphous GBs (Fig. 6).

Following Bobylev *et al.* [95,103], consider a nanocrystalline ceramic solid consisting of nanoscale grains divided by GBs and containing a long and flat mode I crack of length l. Let the crack intersect the boundary at the point distant by r_0 ($r_0 << l$) from the nearest triple junction (Fig. 6). Also, let θ denote the angle between the crack plane and the amorphous intergranular boundary (see Fig. 6). The local stresses near the crack tip in the solid under a tensile load initiate intergrain sliding that results in formation of an immobile dislocation at the nearest triple junction. The dislocation shields the crack tip and thus increases fracture toughness.

Bobylev *et al.* [95,103] have calculated the effect of the intergrain-sliding-produced dislocation at a GB or amorphous intergranular boundary (Fig. 6) on the fracture toughness K_{IC} of a nanocrystalline solid. The dependences of the ratio K_{IC}/K_{IC}^{σ} (where K_{IC}^{σ} is the fracture toughness for brittle fracture, as above) on the angle θ, for $r_0 = 5$ nm, are presented in Fig. 7a, for nanocrystalline 3C-SiC. From this figure it follows that the local fracture toughness K_{IC} reaches its maximum value when the boundary plane (and thereby the Burgers vector of the dislocation) makes the angle of around 70° with the direction of crack growth. This is related to the fact that the shear stress acting in the boundary plane is maximum when the plane makes the angle ≈70° with the direction of crack growth. The dependence of K_{IC} on the distance r_0 between the dislocation and the crack tip, for $\theta = 70^{\circ}$, is presented in Fig. 7b. From this figure it follows that at $r_0 = 1$ nm, disloca-

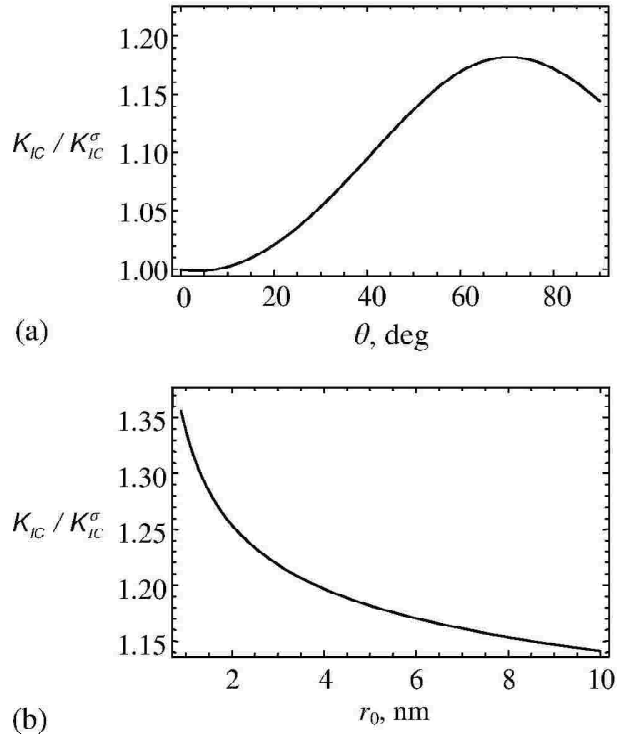

Fig. 7. Dependence of the ratio K_{IC}/ K_{IC}^{σ} in the case of edge dislocation located near crack tip in 3*C*-SiC on (a) angle θ made by the Burgers vector (or boundary plane) with crack growth direction, for r_0 = 5 nm; and (b) distance r_0 between the crack tip and the dislocation, for θ = 70°. Reproduced from [95], with permission.

tion formation leads to the increase of K_{IC} by ≈30%. This effect is significant, but the increase in K_{IC} rapidly falls with increasing r_0. A similar analysis (combined from the analysis of lattice dislocation emission from crack tips in nanocrystalline solids originally performed in works [74,75]) has also been later performed in paper [106].

Now consider the situation where the nanocrystalline solid is strained at a higher temperature ($T>T_{GBD}$), at which GB diffusion is activated but grain growth is suppressed. In this case, GB sliding can be accommodated by GB dislocation climb (Fig. 8). At the first stage of the accommodation, a triple junction dislocation (produced by intergrain sliding (Fig. 8b) climbs along a GB adjacent to the triple junction (Fig. 8c). Then, a new dislocation is formed due to intergrain sliding at the triple junction located near the crack tip, and, as a result, the crack tip blunts (Fig. 8d). The processes of GB dislocation climb and intergrain-sliding-produced formation of GB dislocations consequently occur resulting in dramatic blunting of the crack (Figs. 8c–8f).

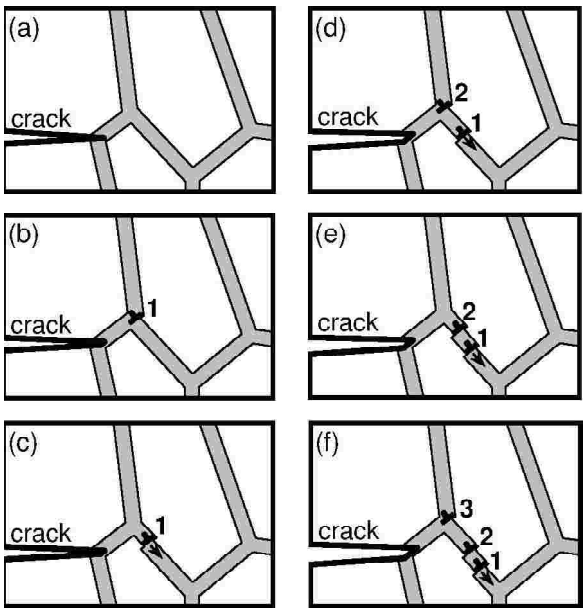

Fig. 8. GB sliding is accommodated through climb of grain boundary dislocations. GB sliding near a crack tip produces triple junction dislocations. These dislocations climb away, in which case GB sliding is enhanced and leads to the blunting of the crack. Reproduced from [103]. Copyright 2010, with permission from Elsevier.

Crack blunting in the course of plastic deformation leads to an increase in the fracture toughness of the nanocrystalline solid. The expression for the fracture toughness K_{IC}^{*} in the case of crack blunting associated with accommodated GB sliding is

as follows [103]:

$$K_{IC}^{*} = \max\left\{\frac{\pi\sigma_p^2 b^4 D_{GB} f(\theta)\sin\theta}{8d^2\sqrt{2\pi d}kT\dot{\varepsilon}}\varepsilon, \sqrt{4G\gamma/(1-\nu)}\right\}, \quad (17)$$

where

$$f(\theta) = \int_0^1 \left(u^2+1\right)^{-1/4}\cos\left(\theta_0/2\right)\left[1+\sin\left(\theta_0/2\right)\sin\left(2\theta-3\theta_0/2\right)\right]\mathrm{d}u, \quad (18)$$

$\theta_0 = \theta$ - arctan$u$, σ_p is the cohesive strength, D_{GB} is the GB diffusion coefficient, d denotes grain size, $b \approx 0.1$ nm is the magnitude of the Burgers vector of GB dislocations, ε is plastic strain, $\dot{\varepsilon}$ specifies strain rate, k is the Boltzmann constant, and T designates absolute temperature.

The dependences of fracture toughness K_{IC}^{*} on grain size d at various temperatures have been calculated in paper [103], for the case of nanocrystalline Al. However, apparently, the qualitative results given by these dependences can also be extended to the case of nanocrystalline ceramics. It appeared that fracture toughness in the case of accommodated GB sliding dramatically (3 to 5 times) increases as the grain size decreases by a factor of 1.5 or the temperature increases by 30 degrees. The effect of crack blunting on fracture toughness K_{IC}^{*} is essential only in the case of small grain sizes (that is, in the situation where grain size is smaller than a critical size d_c). At $d = d_c$ fracture toughness approaches its lowest value K_{IC}^{σ} that corresponds to the case of brittle fracture and does not alter with a further increase in the grain size d. The reason is that with an increase in grain size d, GB dislocation climb becomes too slow to fully accommodate intergrain sliding and can no more promote fast crack blunting and associated increase in fracture toughness K_{IC}^{*}.

Another mechanism of fracture toughness enhancement in nanocrystalline ceramics is associated with rotational deformation, that is, deformation accompanied by a change in the orientation of crystal planes in grains. Rotational deformation can occur under the action of local shear stresses in the vicinities of crack tips and results in their partial relaxation that increases fracture toughness.

Within model [107], special rotational deformation in a nanograin occurs under the action of the applied stress through the formation of immobile disclinations located in the triple junctions of the boundaries of this nanograin (Fig. 9). In the course of rotational deformation disclination strength increases due to GB sliding and diffusion (Fig. 9). GB sliding is realized via glide of GB dislocations that form and GBs AB and CD and slip along these GBs under the action of the applied load. Simultaneously, GB diffusion induces GB dislocation climb along GBs AC and BD (Fig. 9). As a result, at the GBs AC and BD two dislocation walls of opposite signs are formed. These walls of edge dislocations can be approximated as a quadrupole of wedge disclinations [107] situated at the triple junctions A, B, C, and D (Fig. 9).

Within the model under consideration, Morozov *et al*. [107] have calculated the critical stress intensity factor (created by the remote tensile load) for crack growth in the presence of rotational deformation in a rectangular nanograin near a crack tip. Fracture toughness was calculated through averaging of the critical stress intensity factor over various orientations and aspect ratios of grain side lengths. The calculations [107] demonstrated that the ratio K_{IC}/K_{IC}^{σ} of the fracture toughness K_{IC} in the presence of rotational deformation to the toughness K_{IC}^{σ} of brittle fracture does not depend on materials parameters and is approximately equal to 1.12. That is, rotational deformation can increase facture toughness by approximately 12%. Just the same analysis of fracture toughness (but without averaging over various orientations and aspect ratios of grain sides) was later performed in work [108].

4.7. Cooperative grain boundary sliding and migration process as a toughening mechanism

One more mechanism of fracture toughness enhancement in nanocrystalline ceramics has been proposed in work [109]. This mechanism represents GB sliding accommodated by GB migration [110]. In this case the defects created by GB sliding are partially accommodated by the defects created in the course of GB migration. The geometry of this deformation mechanism is shown in Fig. 10. (Note that Fig. 1 of paper [109] describing the geometry of this mechanism contains a mistake in crack tip location. Analysis in work [109] is performed for the geometry shown in Fig. 10 of the present paper.)

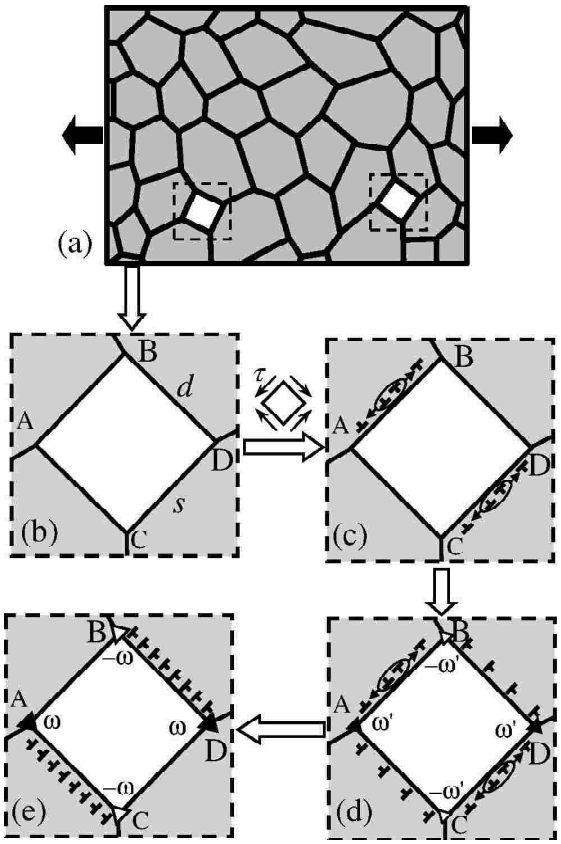

Fig. 9. Rotational deformation in model square grains of a nanocrystalline specimen (schematically). (a) Tensile deformation of a nanocrystalline specimen. General view. (b)–(e) Rotational deformation in a nanograin occurs through slip and climb of GB dislocations and results in the formation of a quadrupole of immobile disclinations (triangles) whose strengths gradually increase during the formation process. Reproduced from [107], with permission from Elsevier.

Fig. 10a depicts a two-dimensional section of a deformed nanocrystalline specimen. Within the model [109,110], GB sliding occurs under the applied shear stress and transforms the initial configuration I of GBs (Fig. 10b) into configuration II (Fig. 10c). GB sliding is assumed to be accommodated, in part, by emission of lattice dislocations from triple junctions (Fig. 10c). Besides, following [111,112], GB sliding results in the formation of a dipole of wedge disclinations A and C in configuration II (Fig. 10c) characterized by strengths $\pm\omega$, whose magnitude ω is equal to the tilt misorientation of the GB AB. The disclination dipole AC has an arm (the distance between the disclinations) equal to the magnitude x of the relative displacement of grains (Fig. 10c).

We further assume [109] that, in parallel with GB sliding, stress-driven GB migration occurs as well, so that the stress fields of defects created by GB sliding are, in part, accommodated by the defects created by GB migration. In the case shown in Fig. 10, the migration of the grain boundary AB into another position DE (by a distance y) results in the formation of a quadrupole of wedge disclinations with the strengths $\pm\omega$ at the points A, B, D, and E [109]. The disclination with the strength $+\omega$ appearing at the point A due to GB sliding and the disclination with the strength $-\omega$ appearing at the same point due to GB migration annihilate. The annihilation results in the disclination configuration shown in Fig. 10d. Thus, the cooperative GB sliding and migration process transforms the initial configuration I (Fig. 10b) into the final configuration III (Fig. 10d) characterized by two disclination dipoles CD and BE (Fig. 10d).

The calculations performed in [109] for nanocrystalline Ni, for $\varphi = 2\pi/3$, $d = 15$ nm, $p = 0$ and various values of ω, has given the following results. It appeared that the length x of GB sliding has an equilibrium value (corresponding to an energy minimum) at any values of ω. At the same time, the equilibrium length of GB migration has a nonvanishing value only at $\omega > \omega_c$, where $\omega_c \approx 21°$ at $K_{IC} = K_{IC}^{\sigma}$. At

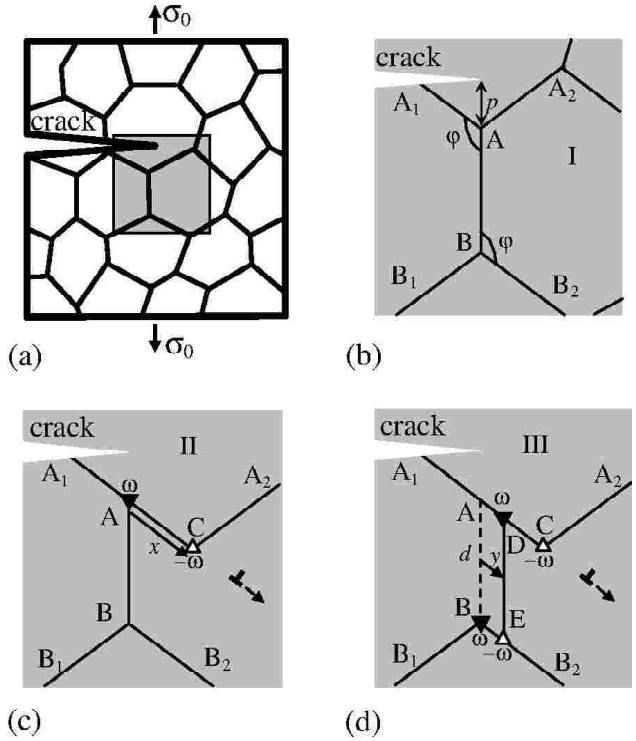

Fig. 10. Grain boundary deformation processes in nanocrystalline specimen near a crack tip. (a) General view. (b) Initial configuration I of grain boundaries. (c) Configuration II results from pure grain boundary sliding. Dipole of disclinations AC is generated due to grain boundary sliding. (d) Configuration III results from cooperative grain boundary sliding and migration process. Two disclination dipoles CD and BE are generated due to this cooperative process. Reproduced from [109], with a modification in figure (a) described in the text. Copyright 2011, with permission from Elsevier.

$\omega < \omega_c$ the equilibrium length of GB migration equals zero. This means that the cooperative GB sliding and migration are energetically favored if the absolute value ω of the disclination strength exceeds a critical value, which depends on the applied load (more precisely, on the stress intensity factor created by the applied load). If the disclination strength ω is smaller than the critical value, GB sliding without GB migration is energetically favored. Similar results have been obtained for nanocrystalline ceramic 3C-SiC.

Also, Ovid'ko *et al*. [109] calculated and analyzed the effect of the cooperative GB sliding and migration on the fracture toughness of nanocrystalline solids. The calculation for nanocrystalline 3C-SiC with grain size d = 15 nm provided the following results. The ratio K_{IC}/K_{IC}^{σ} of the fracture toughness K_{IC} in the presence of GB sliding and migration to the fracture toughness K_{IC}^{σ} for brittle fracture at ω = 45°, 30°, and 15° is equal to 1.68, 1.96, and 3.40, respectively, for an intragrain crack, and to 1.63, 1.90, and 3.65, respectively, for a GB crack. Thus, the mechanism suggested in [109] can dramatically increase the fracture toughness of nanocrystalline ceramics.

Besides, Ovid'ko *et al*. [109] have calculated the dependences of fracture toughness in the presence

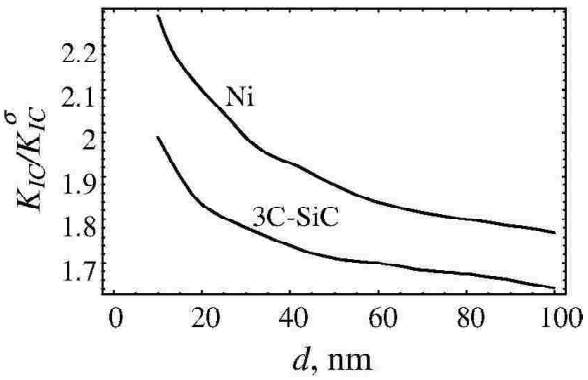

Fig. 11. Normalized critical stress intensity factor K_{IC}/K_{IC}^{σ} vs grain size d, in the case of a grain boundary crack in nanocrystalline Ni and 3C-SiC. Reproduced from [109]. Copyright 2011, with permission from Elsevier.

of cooperative GB sliding and migration on grain size. The dependences K_{IC}/K_{IC}^{σ} on grain size d for nanocrystalline Ni and nanocrystalline ceramic 3C-SiC are shown in Fig. 11 for $\omega = 30°$. As follows from Fig. 11, for 3C-SiC an increase in grain size from 10 to 100 nm leads to a decrease of the ratio K_{IC}/K_{IC}^{σ} from 1.99 to 1.64. This tendency allows us to conclude that the cooperative GB sliding and migration mechanism is most effective in fracture toughness enhancement precisely in nanocrystalline ceramics at finest grain sizes.

Concluding remarks. Thus, the review in the present section demonstrates that various specific toughening micromechanisms associated with nanoscale plastic deformation in nanoceramics can increase their fracture toughness via a decrease of local stresses near crack tips. The micromechanisms associated with GB deformation are expected to be most effective in fracture toughness enhancement in nanoceramics.

5. SUMMARY

Thus, we have reviewed experimental data, computer simulations, and theoretical models concerning both crack growth processes and toughening mechanisms/strategies in nanocrystalline ceramics. The key conclusions based on the review are as follows. The structural features and phase content cause significant effects on crack growth in nanoceramics. The toughening mechanisms in nanoceramics comprise both the conventional mechanisms typical of ceramics with various grain sizes and the mechanisms characteristic of precisely nanocrystalline ceramics. The conventional toughening mechanisms – ductile phase toughening, fiber toughening and transformation toughening – have their analogs operating in microcrystalline ceramics [10]. The most effective approaches to create ceramic nanocomposites with high fracture toughness appear to be the implantation of single-wall carbon nanotubes in ceramics or of the use of nanocrystalline zirconia as one of the components of ceramic nanocomposites. The toughening micromechanisms based on nanoscale plastic flow modes specific for nanocrystalline materials include, in particular, GB sliding, the rotations of crystal planes in nanograins, GB migration and GB diffusion. The results of the reviewed theoretical models/calculations demonstrate that the strongest effect on the fracture toughness of nanoceramics is due to GB sliding and cooperative GB sliding and migration. These plastic deformation modes operating near crack tips can increase the fracture toughness of nanoceramics by a factor of 2 to 3, compared to the toughness of brittle fracture.

ACKNOWLEDGEMENTS

The work was supported, in part, by the Russian Ministry of Science and Education (Contract 14.740.11.0353) and the Russian Academy of Sciences Program "Fundamental studies in nanotechnologies and nanomaterials".

REFERENCES

[1] J.D. Kuntz, G.-D. Zhan and A.K. Mukherjee // *MRS Bull.* **29** (2004) 22.
[2] A. Mukhopadhyay and B. Basu // *Int. Mater. Rev*. **52** (2007) 257.
[3] R.A. Andrievski and A.M. Glezer // *Physics – Uspekhi* **52** (2009) 315.
[4] A.V. Sergueeva, D.M. Hulbert, N.A. Mara and A.K. Mukherjee, In: *Nanostructured Materials*, ed. by G. Wilde (Elsevier, 2008), p. 127.
[5] S.C. Tjong and H. Chen // *Mater. Sci. Eng. R* **45** (2004) 1.
[6] C.C. Koch, I.A. Ovid'ko, S. Seal and S. Veprek, *Structural Nanocrystalline Materials: Fundamentals and Applications* (Cambridge University Press, Cambridge, 2007).
[7] M.A. Morris and M. Leboeuf // *Mater. Sci. Eng. A* **224** (1997) 1.
[8] C.C. Koch, D.G. Morris, K. Lu and A. Inoue // *MRS Bullet.* **24** (1999) 54.
[9] G.-D. Zhan, J.D. Kuntz, J. Wan and A.K. Mukherjee // *Nature Mater.* **2** (2003) 38.
[10] G.-D. Zhan and A.K. Mukherjee // *Int. J. Appl. Ceram. Technol.* 1 (2004) 161.
[11] Z. Xia, L. Riester, W.A. Curtin, H. Li, B.W. Sheldon, J. Liang, B. Chang and J.M. Xu // *Acta Mater.* **52** (2004) 931.
[12] S. Bhaduri and S.B. Bhaduri // *Nanostruct. Mater.* **8** (1997) 755.
[13] A.A. Kaminskii, M.Sh. Akchurin, R.V. Gainutdinov, K. Takaichi, A. Shirakava, H. Yagi, T. Yanagitani and K. Ueda // *Crystallography Reports* **50** (2005) 869.
[14] Y. Zhao, J. Qian, L.L. Daemen, C. Pantea, J. Zhang, G.A. Voronin and T.W. Zerda // *Appl. Phys. Lett.* **84** (2004) 1356.
[15] Y.T. Pei, D. Galvan D and J.Th.M. De Hosson // *Acta Mater.* **53** (2005) 4505.

[16] R.W. Siegel, S.K. Chang, B.J. Ash, J. Stone, P.M. Ajayan, R.W. Doremus and L.S. Schadler // *Scr. Mater.* **44** (2001) 2061.
[17] H. Liu, C. Huang, X. Teng and H. Wang // *Mater. Sci. Eng. A* **487** (2008) 258.
[18] X. Zhou, D.M. Hulbert, J.-D. Kuntz, R.K. Sadangi, V. Shukla, B.H. Kear and A.K. Mukherjee // *Mater. Sci. Eng. A* **394** (2005) 353.
[19] G.-D. Zhan, J.E. Garay and A.K. Mukherjee // *Nano Lett.* **5** (2005) 2593.
[20] X. Xu, T. Nishimura, N. Hirosaki, R.-J. Xie, Y. Yamamoto and H. Tanaka // *Acta Mater.* **54** (2006) 255.
[21] D.M. Hulbert, D. Jiang, J.D. Kuntz, Y. Kodera and A.K. Mukherjee // *Scr. Mater.* **56** (2007) 1103.
[22] A. Dominguez-Rodriguez, D. Gomez-Garcia, E. Zapata-Solvez, J.Z. Chen and R. Chaim // *Scr. Mater.* 56 (2007) 89.
[23] J.C.M. Li // *J. Appl. Phys*. **33**, 2958 (1962).
[24] M.Yu Gutkin, K.N. Mikaelyan and I.A. Ovid'ko // *Scr. Mater.* 58, 850 (2008).
[25] K. Niihara, A. Nakahira and T. Sekino, In: *Nanophase and Nanocomposite Materials*, *MRS Symp. Proc*., ed. by S. Kormaneni, J.C. Parker and G.J. Thomas (MRS, Pittsburg, 1993), p. 405.
[26] K. Niihara // *J. Ceram. Soc. Jpn.* **99** (1991) 974.
[27] K. Niihara, A. Nakahira, In: *Advanced Structural Inorganic Composites*, ed. by P. Vincenzini (Elsevier, Amsterdam, 1991), p. 637.
[28] R.A. Andrievski, In: *Functional Gradient Materials and Surface Layers Prepared by Fine Particles Technology*, ed. by M.-I. Baraton and I. Uvarova (Kluwer, Dordrecht, 2002), p. 17.
[29] S. Jiao, M.L. Jenkins and R.W. Davidge // *Acta Mater.* **5** (1997) 149.
[30] M.Yu. Gutkin and I.A. Ovid'ko // *Scripta Mater.* **59** (2008) 414.
[31] P.J.F. Harris // *Int. Mater. Rev.* **49** (2004) 31.
[32] N.P. Padture // *Adv. Mater.* **21** (2009) 1.
[33] A. Peigney, C. Laurent, F. Dobigeon and A. Rousset // *J. Mater. Res.* **12** (1997) 613.
[34] R.Z. Ma, J. Wu, B.Q. Wei, J. Liang and D.H. Wu // *J. Mater. Sci.* **33** (1998) 5243.
[35] T. Seeger, T. Köhler, T. Frauenheim, N. Grobert, M. Rühle, M. Terrones and G. Seifert // *Chem. Commun* (2002) 34.
[36] P. Vincent, A. Brioude, C. Journet, S. Rabaste, S.T. Purcell, J. Le Brusq and J.C. Plenet // *J. Non-Cryst. Sol.* **311** (2002) 130.
[37] X. Wang, N.P. Padture and H. Tanaka // *Nat. Mater.* **3** (2004) 539.
[38] J. Sun, L. Gao, M. Iwasa, T. Nakayama and K. Niihara // *Ceram. Int.* **31** (2005) 1131.
[39] G.-D. Zhan and A.K. Mukherjee // *Rev. Adv. Mater. Sci.* **10** (2005) 185.
[40] Z. Burghard, D. Schon, J. Bill and F. Aldinger // *Int. J. Mater Res.* **97** (2006) 1667.
[41] J.P. Fan, D.M. Zhuang, D.Q. Zhao, G. Zhang, M.S. Wu, F. Wei and Z.J. Fan // *Appl. Phys. Lett.* **89** (2006) 121910.
[42] T. Wang, Z. Iqbal and S. Mitra // *Carbon* **44** (2006) 2804.
[43] A.L. Vasiliev, R. Poyato and N.P. Padture // *Scr. Mater.* **56** (2007) 461.
[44] D. Jiang, K. Thomson, J.D. Kuntz, J.W. Ager and A.K. Mukherjee // *Scr. Mater.* **56** (2007) 959.
[45] E.L. Corral, J. Cesarano, A. Shyam, E. Lara-Curzio, N. Bell, J. Stuecker, N. Perry, M. Di Prima, Z. Munir, J. Garay and E.V. Barrera // *J. Am. Ceram. Soc.* **91** (2008) 3129.
[46] P.A. Calvert // *Nature* **399** (1999) 210.
[47] B.A. Cottom and M.J. Mayo // *Scr. Mater.* **34** (1996) 809.
[48] A. Bravo-Leon, Y. Morikawa, M. Kawahara and M.J. Mayo // *Acta Mat.* **50** (2002) 4555.
[49] O. Vasylkiv, Y. Sakka and V. Skorokhod // *Key Engineering Materials* **317** (2006) 615.
[50] L. Shu-quan, T. Xiao-ping, L. Shao-qiang and T. Yan // *Journal of Central South University of Technology* **14** (2007) 1.
[51] B. Zhao, B.Y. Du and T.L. Duan, In: *Advanced Design and Manufacture to Gain a Competitive Edge*, ed. by X.-T. Yan, C. Jiang and B. Eynard (Springer, London, 2008), p. 215.
[52] H. Awaji, S.-M. Choi and E. Yagi // *Mech. Mater.* **34** (2002) 411.
[53] S.-M. Choi and H. Awaji // *Sci. Technol. Adv. Mater.* **6** (2005) 2.
[54] R.W. Williams, *Mechanical Behaviour of Ceramics* (Cambridge University Press, London, 1979).
[55] H. Gleiter // *Acta Mater.* **48** (2000) 1.
[56] S. Veprek and A.S. Argon // *J. Vac. Sci. Technol.* **20** (2002) 650.
[57] K.S. Kumar, S. Suresh and H. Van Swygenhoven // *Acta Mater.* **51** (2003) 5743.
[58] W.W. Milligan, I*n: Comprehensive structural integrity*, ed. by I. Milne, R.O. Ritchie and B.

Karihaloo (Elsevier, Amsterdam, 2003), p. 529.
[59] R.Z. Valiev // *Nature Mater.* **3** (2004) 511.
[60] M.Yu. Gutkin and I.A. Ovid'ko, *Plastic Deformation in Nanocrystalline Materials* (Springer, Berlin-Heidelberg-N.Y., 2004).
[61] B.Q. Han, E. Lavernia and F.A. Mohamed // *Rev. Adv. Mater. Sci.* **9** (2005) 1.
[62] I.A. Ovid'ko // *Int. Mater. Rev.* **50** (2005) 65.
[63] I.A. Ovid'ko // *Rev. Adv. Mater. Sci.* **10** (2005) 89.
[64] D. Wolf, V. Yamakov, S.R. Phillpot, A.K. Mukherjee and H. Gleiter // *Acta Mater.* **53** (2005) 1.
[65] M.A. Meyers, A. Mishra and D.J. Benson // *Progr. Mater. Sci.* **51** (2006) 427.
[66] C.S. Pande and K.P. Cooper // *Progr. Mater. Sci.* **54** (2009) 689.
[67] I. Szlufarska, A. Nakano and P. Vashishta // *Science* **309** (2005) 911.
[68] J.C.M. Li // *Phys. Rev. Lett.* **96** (2006) 215506.
[69] S.V. Bobylev, M.Yu. Gutkin and I.A. Ovid'ko // *Acta Mater.* **52** (2004) 3793.
[70] V.A. Pozdnyakov and A.M. Glezer // *Phys. Solid State* **47** (2005) 817.
[71] T. Shimokawa, M. Tanaka, K. Kinoshita and K. Higashida // *Phys. Rev. B* **83** (2011) 214113.
[72] N. Tsuji, S. Okuno, Y. Koizumi and Y. Minamino // *Mater. Trans.* **45** (2004) 2272.
[73] M. Tanaka, N. Fujimoto and K. Higashida // *Mater. Trans.* **49** (2008) 58.
[74] I.A. Ovid'ko and A.G. Sheinerman // *Scripta Mater.* **60** (2009) 627.
[75] I.A. Ovid'ko and A.G. Sheinerman // *Acta Mater.* **58** (2010) 5286.
[76] M.D. Sangid, G.J. Pataky, H. Sehitoglu, R.G. Rateick, T. Niendorf and H.J. Maier // *Acta Mater.* **59** (2011) 7340.
[77] I.A. Ovid'ko, A.G. Sheinerman and E.C. Aifantis // *Acta Mater.* **56** (2008) 2718.
[78] N.F. Morozov, I.A. Ovid'ko, A.G. Sheinerman and E.C. Aifantis // *Mater. Phys. Mech.* **8** (2009) 155, In Russian.
[79] M.Yu. Gutkin and I.A. Ovid'ko // *Appl. Phys. Lett.* **87** (2005) 251916.
[80] M. Dao, L. Lu, R.J. Asaro, J.Th.M. De Hosson and E. Ma // *Acta Mater.* **55** (2007) 4041.
[81] J.C.M. Li // *Surf. Sci.* **31** (1972) 12.
[82] A.E. Romanov and V.I. Vladimirov, In: *Dislocations in Solids*, ed. by F.R.N. Nabarro (North Holland, Amsterdam, 1992), vol. 9, p. 191.
[83] W. Bollmann // *Philos. Mag. A* **49** (1984) 73.
[84] W. Bollmann // *Philos. Mag. A* **57** (1988) 637.
[85] G. Dimitrakopulos, P. Komminou, T. Karakostas and R.C. Pond // *Interface Sci.* **7** (1999) 217.
[86] P. Klimanek, V. Klemm, A.E. Romanov and M. Seefeldt // *Adv. Eng. Mater.* **3** (2001) 877.
[87] R.G. Irwin // *J. Appl. Mech.* **24** (1957) 361.
[88] Mechanics of fracture and strength of materials (ed. by V.V. Panasyuk). (Naukova dumka, Kiev, 1988), vol. 2, In Russian.
[89] Z. Ding, S. Zhou and Y. Zhao // *Phys. Rev. B* **70** (2004) 184117.
[90] M.Yu. Gutkin, I.A. Ovid'ko and N.V. Skiba // *Philos. Mag.* **88** (2008) 1137.
[91] M.F. Ashby and R.A. Verall // *Acta Metall.* **21** (1973) 149.
[92] W. Yang and H.T. Wang // *J. Mech. Phys. Solids* **54** (2004) 875.
[93] W. Yang and H.T. Wang // *Int. J. Sol. Struct.* **45** (2008) 3897.
[94] F. Yang and W. Yang // *J. Mech. Phys. Solids* **57** (2009) 305.
[95] S.V. Bobylev, A.K. Mukherjee, I.A. Ovid'ko and A.G. Sheinerman // *Rev. Adv. Mater. Sci.* **21** (2009) 99.
[96] Y. Mo and I. Szlufarska // *Appl. Phys. Lett.* **90** (2007) 181926.
[97] J. Crampon, R. Duclos and N. Rakotoharisoa // *J. Mater. Sci.* **25** (1990) 1203.
[98] R.D. Nixon, D.A. Koester, S. Chevacharoenkul and R.F. Davis // *Sci. Technol*. **37** (1990) 313.
[99] J. Crampon, R. Duclos and N. Rakotoharisoa // *J. Mater. Sci.* **28** (1993) 909.
[100] S.Y. Yoon, T. Akatsu and E. Yasuda // *J. Mater. Sci.* **32** (1997) 3813.
[101] J.-L. Besson, M. Mayne, D. Bahloul-Hourlier and P. Goursat // *J. Eur. Ceram. Soc*. **18** (1998) 1893.
[102] K.J. Yoon, S.M. Wiederhorn and W.E. Luecke // *J. Am. Ceram. Soc.* **83** (2000) 2017.
[103] S.V. Bobylev, A.K. Mukherjee, I.A. Ovid'ko and A.G. Sheinerman // *Int. J. Plasticity* **26** (2010) 1629.
[104] V V. Volterra // *Ann. Sci. Ecole Norm. Sup.* **24** (1907) 401.
[105] J.P. Hirth and J. Lothe, *Theory of Dislocations* (Wiley, New York, 1982).

[106] Y. Liu, J. Zhou, L. Wang, S. Zhang and Y. Wang // *Mater. Sci. Eng. A* **528** (2011) 4615.
[107] N.F. Morozov, I.A. Ovid'ko, A.G. Sheinerman and E.C. Aifantis // *J. Mech. Phys. Solids* **58** (2010) 1088.
[108] Y. Liu, J. Zhou, T.D. Shen and D. Hui // *Mater. Sci. Eng. A* **528** (2011) 7684.
[109] I.A. Ovid'ko, A.G. Sheinerman and E.C. Aifantis // *Acta Mater.* **59** (2011) 5023.
[110] S.V. Bobylev, N.F. Morozov and I.A. Ovid'ko // *Phys. Rev. Lett.* **105** (2010) 055504.
[111] I.A. Ovid'ko and A.G. Sheinerman // *Appl. Phys. Lett.* **90** (2007) 171927.
[112] I.A. Ovid'ko and A.G. Sheinerman // *Acta Mater.* **57** (2009) 2217.